Version of Record: https://www.sciencedirect.com/science/article/pii/S0377027319302665
Manuscript_cdf923adfef7bba85d89cef7602ee178

A robust, low-cost and well-calibrated infrasound sensor for volcano monitoring

Jacques Grangeon[1], Philippe Lesage[1,*]

[1] Université Grenoble Alpes, Université Savoie Mont Blanc, CNRS, IRD, IFSTTAR, ISTerre, 38000 Grenoble, France.

* Corresponding author. lesage@univ-smb.fr

ISTerre, Université Savoie Mont Blanc, Campus scientifique, 73376 Le Bourget-du-Lac cedex

Abstract

Volcano acoustic signals contain valuable information on shallow magmatic and hydrothermal processes. In some cases, the detection of acoustic waves is the only clear evidence of the occurrence of volcanic explosions. Their study is thus complementary to that of seismic signals. For this reason, acoustic sensors are more and more frequently integrated in volcano monitoring systems as well as in temporary instrumental deployments. We have developed a broadband, robust and low-cost infrasound sensor designed for the detection and analysis of acoustic waves on volcanoes. It is based on a microelectromechanical differential pressure transducer (MEMS). The reference pressure is balanced with the atmospheric pressure through a pneumatic high-pass filter. Its low corner frequency, usually set to 60 mHz, can be adjusted from a few to tens of mHz. Its amplitude range is ± 240 Pa and its sensitivity is 20 mV Pa^{-1}, with a noise level less than 0.05 Pa RMS. The power consumption is 42 mW (3.5 mA with 12 V voltage). A direct output of the MEMS also provides a signal with sensitivity of about 500 µV Pa^{-1} and range ± 1245 Pa. This sensor is not sensitive to mechanical vibrations. The instrumental response of each infrasound sensor is carefully measured from 1 mHz to more than 100 Hz using two specially designed calibration systems which deliver sinusoidal pressure variations. The mechanical elements of the sensor are produced by 3D printer and filled with epoxy resin which guarantees high robustness in the aggressive environment of most volcanoes. The sensor dimensions (26x45x80 mm) and weight (100 g) makes it very easy to handle and install.

Keywords: Instrumentation, infrasound, sensor, volcano monitoring

1. Introduction

A large variety of volcanic processes produce perturbations of the atmosphere that propagate as acoustic waves. These include sudden or continuous emissions of material, in solid, liquid or gaseous state, at the Earth's surface, mass transfers associated with dome collapse, pyroclastic density currents, or rockfalls, and seismic ground vibrations coupled with the air. The frequency of these atmospheric perturbations can be in the audio range (> 20 Hz and < 20 000 Hz), but strong acoustic energy is often observed in the infrasound range, i.e. at frequency lower than 20 Hz (Johnson and Ripepe, 2011; Fee and Matoza, 2013). Therefore, the spectrum of acoustic waves may have components at frequencies smaller and larger than the lower limit of the audible band for human ear. The detection, recording, and analysis of the infrasonic signals produced by volcanoes highlight the physical processes related with volcanic activity and provide important information such as mass flux and velocity of gas emission, over-pressure associated with explosions, and source location (Johnson and Ripepe, 2011; Fee and Matoza, 2013; Garcés et al., 2013). This information can be quantitative and of physical significance if the sensors used are calibrated. Since low frequency acoustic waves propagate in the atmosphere with little attenuation, they can be observed and analyzed at long distances from the source and even all around the Earth for large explosions (Delclos et al., 1990; Le Pichon et al., 2010).

Volcano monitoring is primarily based on the observation of seismic activity with networks of seismometers deployed on or close to the edifices. An important task in volcano observatories is to detect and classify the events according to pre-defined classes such as volcano-tectonic event, long-period event, tremor, or explosion. However, in many cases, it is difficult to identify and separate LP events from explosion quakes, because both types of event share common temporal and spectral features. Thus, when there are no visual observations due to night or cloudy conditions, volcanic explosions may pass unnoticed when using only seismic methods. In this kind of situation, the use of infrasound sensors to complement the monitoring system may be of invaluable help for detecting and discriminating explosions (De Angelis et al., 2012). Furthermore, the deployment of arrays of at least 3 or 4 infrasound sensors is very useful to improve the detection of small events, to determine back-azimuth to locate their source and to separate the signals according to their origin (Johnson et al., 2011). However, although their use tends to rapidly extend, there are still few infrasound sensors available with characteristics well-adapted for research and monitoring purposes in volcanology.

We have developed an infrasound sensor suited to the conditions found on volcanoes and easy to integrate in monitoring networks. The sensor has the following specifications: a low noise level and a dynamic range designed for detecting small to moderate explosions at a few kilometers from the source; a good resistance to harsh environmental conditions, including rain, humidity, temperature variations, corrosive gas, insolation, and insects; low power consumption and easy connection to most seismic digitizers; large bandwidth with adjustable low corner frequency (typically 60 mHz); precise calibration; low sensitivity to mechanical vibrations; easy installation and possible connection to acoustic noise reducers; small dimensions and weight; low cost. In this paper, we describe the principle of the IST-2018 sensor, the mechanical configuration, the electronic design, and its main features. In order to validate the sensor design, we compare signals of volcanic explosions recorded by our sensor and by a commercial high-precision and high-sensitivity sensor. We also present devices to easily calibrate infrasound sensors from one mHz to several hundred Hz and to test their sensitivity to mechanical vibrations.

2. Choice and principle of infrasound sensor

Infrasounds are perturbations of the atmospheric pressure that can be detected by absolute and differential pressure sensors. The pressure at Earth's surface is about 1000 hPa at sea level and can vary in a range of up to 800 hPa, depending on the altitude and meteorological conditions (Ponceau and Bosca, 2010). On the other side, the smallest detectable perturbations above the background noise are of the order of one mPa, depending on the recording site and the frequency (Bowman et al., 2005; Le Pichon et al., 2010). Thus the dynamic range of an absolute pressure sensor, or micro-barometer, able to measure the full scale of atmospheric pressure and to detect the smallest perturbations must be of the order of 10^8. Such sensors, with high sensitivity and large dynamic range, are difficult and expensive to design and produce from the mechanical, electronic, and digital points of view. Differential sensors compare the instantaneous pressure to a reference value which is an average of the previous atmospheric pressures. They provide a high-pass filtered measure of the pressure, which requires much smaller dynamic range than absolute sensors (Rocard, 1971).

When selecting a type of infrasound sensor for carrying out measurements on volcanoes, high-quality microbarometers, such as the Martec MB2005 and the Chaparral Physics Model 50, that are used in the International Monitoring System of the Comprehensive Nuclear-Test-

Ban Treaty Organization, appear expensive and poorly portable and require complex installation procedures. Some industrial pressure sensors, such as the SETRA270, are poorly suited for applications on volcanoes because of their high noise level, power consumption, and cost. Condenser microphones have interesting sensitivity characteristics but their low frequency response is limited. For example, a high-quality microphone, such the GRAS 40E, has a sensitivity of 50 mV Pa^{-1} and a low cut-off frequency of 3 Hz, while a basic microphone, such as SHURE PGA81, has a sensitivity of 3.8 mV Pa^{-1} and a low cut frequency of 40 Hz. On the other hand, these devices are sensitive to corrosion and cannot operate permanently in the field. Industrial pressure sensors and microphones also require signal conditioning electronics – filters and amplifiers – that are not always delivered by the manufacturers. Nevertheless, some infrasound sensors have already been designed for volcanological studies, such as the Chaparral 60 UHP (http://chaparralphysics.com/model60.html) or the ones developed at the New Mexico Institute of Mining and Technology and at the Boise State University, USA (Marcillo et al., 2012; Anderson et al., 2018).

After exploring the technological solutions presented above, we decided to use a piezo-resistivity differential pressure transducer base on microelectromechanical systems (MEMS) technology (Honeywell NSCDJJN005NDUNV). This transducer is designed for static measurements and thus can work at very low frequency, although it is still sensitive at frequency of several hundreds of Hz. The device measures the pressure difference between the atmosphere and a reference cavity which is connected to the external pressure through a pneumatic filter. We tested several technical solutions for this analog filter and we chose to insert a capillary tube between the reference cavity and the exterior. This tube acts as a small leak that progressively equilibrates the pressures between both sides. The principle of this differential pressure sensor was described by Rocard (1971) and Richiardone (1993) and its physical behavior was studied by Mentink and Evers (2011) and Marcillo et al. (2012).

3. Mechanical configuration

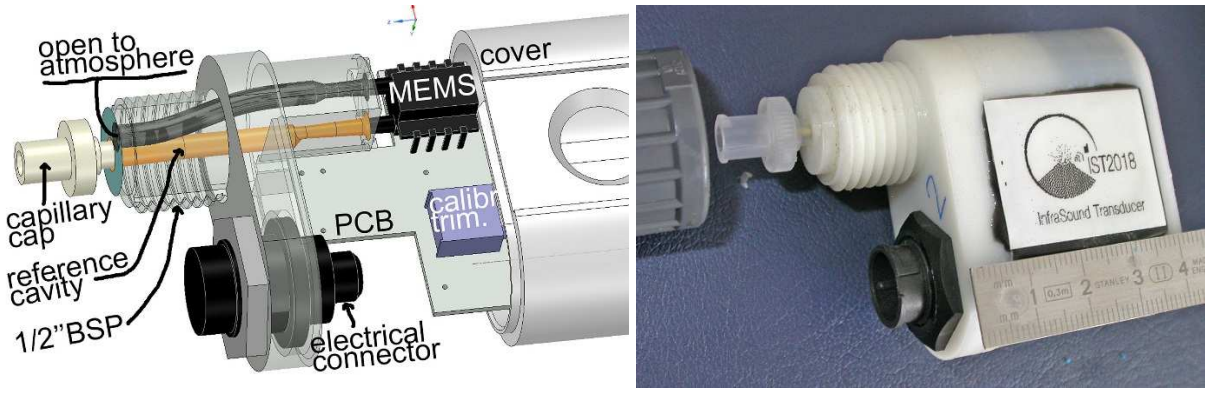

Figure 1. Left panel: block diagram of the infrasound sensor, showing the MEMS, the capillary tube, the reference cavity, the electronic board, and the connector. All these elements are inserted in the packaging displayed on the right side of the picture. Right panel: picture of the sensor.

Figure 1 displays a picture of the sensor packaging and configuration. One side of the differential pressure transducer (MEMS) is directly open to the atmosphere, while the other side is connected through a backing volume and a capillary tube protected, on the atmospheric side, by a hygrophobe Teflon membrane with pore size of 0.45 µm. The length of the capillary tube determines the corner frequency of the pneumatic high-pass filter. For example, we obtain a corner frequency of 55 mHz with a 35 mm-long tube with internal diameter of 65 µm and a backing volume of approximately 230 mm^3. The capillary tube is easily removable. Therefore, it is possible to change it in the field when necessary. The structure and packaging are made in ABS by using a 3D printer. The resulting case contains the MEMS, the backing volume, the capillary tube and the electronic board. The unused volume of this case is filled by epoxy resin before calibration of the sensor. The mechanical parts of the MEMS are also made in plastic. Thus, the design and the material used allow a very good resistance to corrosion and to the aggressive environments that can be found on volcanoes. The small sensor dimensions (26x45x80 mm^3) and weight (~100 g) make it very easy to handle and to install. The atmospheric pressure input and the end of the capillary tube are located in a unique ½" BSP connector which allows an easy link with any noise reducer (Walker and Hedlin, 2010). This connector is equipped with a bug filter.

4. Design of the electronic board

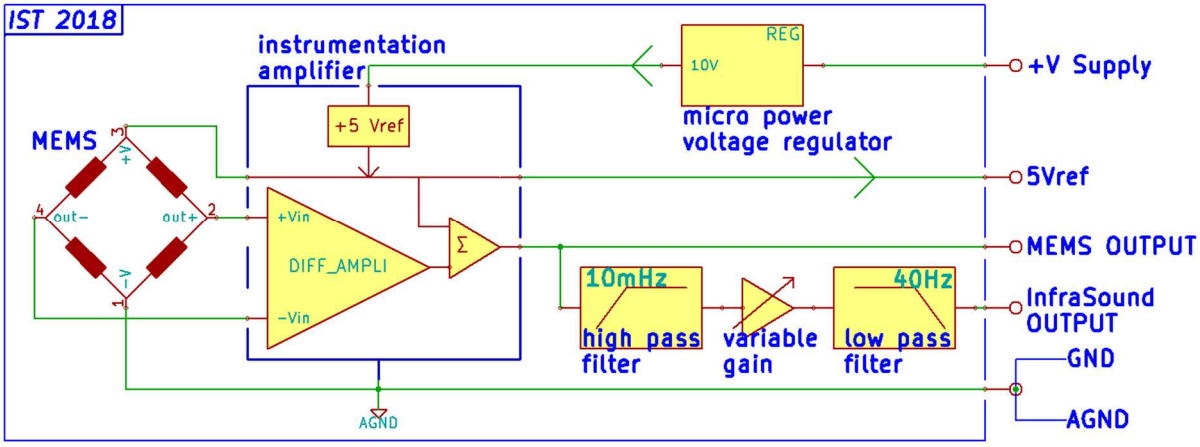

Figure 2. Electronic diagram of the IST-2018 sensor.

Pressure variations produce changes in the piezo-resistive element of the MEMS. The corresponding electrical resistance variations are measured using a Wheatstone bridge. The electronic diagram (figure 2) includes a 10 V micro-power voltage regulator, an instrumentation amplifier with precision voltage reference, a 10 mHz high-pass filter, a variable gain amplifier and a 40 Hz low-pass filter which eliminates high frequency noise. The corner frequencies of these two filters are adjustable by setting the values of their resistors and capacitors when wiring the electronic boards. Together with the pneumatic filter, they allow to define the spectral range of interest. The micro-power voltage regulator delivers a stable 10 V power supply to the electronic components. The instrumentation amplifier excites the bridge and amplifies the electrical variations. All the electronic components were selected in order to lower the power consumption and to minimize the intrinsic noise level. The board, designed with a minimum number of components, includes three outputs. **1)** The '5 Vref' is the precision voltage reference output, accurate to +/-0.5 % with +/-35 ppm/°C drift. **2)** The 'MEMS' output delivers an unfiltered signal with sensitivity of approximately 500 µV Pa^{-1}, depending on the MEMS characteristics. **3)** The 'infrasound' (IS) output delivers a signal filtered by the 10 mHz high-pass filter, which compensates the offset of the sensor, and by the 40 Hz low-pass filter, which reduces the high-frequency noise. The sensitivity, fitted with the variable gain amplifier, is 20 mV Pa^{-1} (+/- 2%). Table 1 summarizes the main features of the IST-2018 sensor.

	IS output	MEMS output
Frequency range	60 mHz* - 40 Hz*	60 mHz* - ~500 Hz*

Sensitivity	20 mV Pa^{-1}	500 µV Pa^{-1}
Amplitude range	± 240 Pa	± 1245 Pa
Background noise (0.06 – 40 Hz)	< 0.05 Pa RMS	< 1 Pa RMS
Dynamic range	> 80 dB	> 68 dB
Power consumption	42 mW (10.2 - 29 V)	
Dimensions and weight	26 x 55 x 80 mm. 100 g	

Table 1. Main features of the IST-2018 infrasound sensor. (*) Adjustable value.

The sensor was designed to be connected to seismic recorders which have often free input channels. The 10 V micro-power voltage regulator powers the electronic sensor in a single mode. Consequently, the signal outputs are strictly positive compared to the sensor ground. The output range is approximately 0 to 10 V; the signal is centered on the 5 V reference. Therefore, the signal can be measured in single mode. It is also possible, and preferable for noise consideration, to use a differential mode in which the 5 Vref is the E- input. In this case, the range is +/-5 V and the common voltage can reach 10 V. With some seismic recorders, such as the 'Nanometrics Taurus', the recorder and sensor supplies must be isolated. For this case, we have developed an optional isolated power source that can supply up to five sensors, at the expense of higher power consumption and noise level. We have also designed a specific adaptor for DataCUBE recorders the input range of which is +/- 2 V.

5. Characterization

If the infrasound signals are used to constrain source physical parameters and to quantify volcanic explosions and activity, they must be recorded by well-calibrated sensors (Fee and Matoza, 2013). The response of the sensors must also be stable over time and their amplitude must be preferably flat in the working frequency range. Usually, the calibration is carried out by installing the sensor in an infrasonic testing chamber in which well-controlled pressure variations are produced (Kromer and McDonald, 2000; Kromer et al., 2007; Marcillo et al., 2012). Because we had no such equipment, we designed a simple calibration system which consists in generating sinusoidal pressure variations with frequency from 1 mHz to hundreds Hz. This system is directly connected to three sensors in parallel: 1) a high quality well-

calibrated sensor used as a reference, 2) a calibrated and unfiltered IST-2018 sensor which is used to measure the phase shift, and 3) the sensor to calibrate. At low frequency, the reference sensor used is a Martec MB2005 microbarometer, the transfer function and sensitivity of which are well-determined. At frequency higher than 5 Hz, a GRAS 40AE microphone is used as a reference instead of the MB2005. For each selected frequency, the sinusoidal pressure variations are recorded by the three sensors. The complex transfer function is obtained point by point by comparing the amplitude and phase of the corresponding signals. Appendix A describes more in detail the calibration system and procedure.

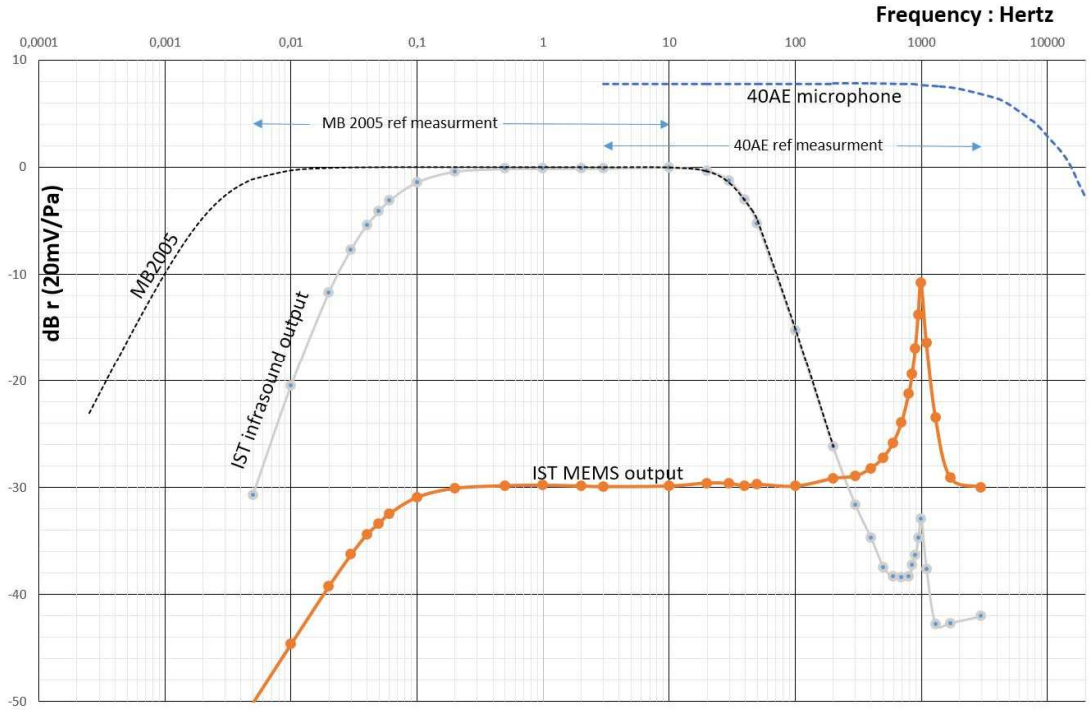

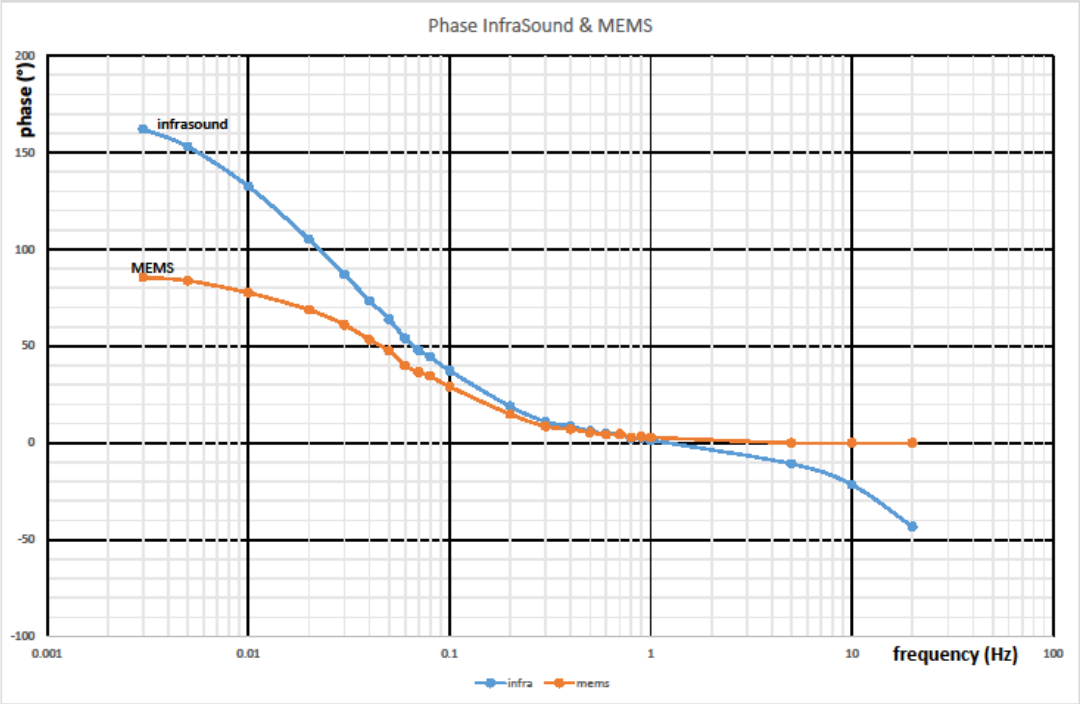

Figure 3. Amplitude (top) and phase (bottom) responses of the IST-2018 for its infrasound (IS – blue) and MEMS (red) outputs. Dots are values measured with the calibration system. Amplitude responses of the MB2005 and the GRAS 40AE microphone are also displayed in top panel for comparison. Double arrows indicate the frequency ranges used for each reference sensor in the calibration procedure.

Figure 3 displays the amplitude and the phase of the transfer function of the two outputs of the IST-2018 sensor. For the IS output, the response is flat from 50 mHz to 40 Hz. The lower corner frequency is that of the pneumatic filter and can be easily modified. We carried out tests with corner frequency as low as 6 mHz. The 'MEMS' output is not low-pass filtered. Its response is also flat up to a few hundred Hz. At 1000 Hz, i.e. outside the normal working frequency band, a peak appears in the amplitude curve of both outputs. It is probably due to a resonance of the MEMS itself. The linearity is obtained by comparing the amplitudes of the pressure variations recorded by the MB2005 and the IST-2018 sensors (figure 4). The mean relative deviation from linearity is 0.66 % between 1.2 and 220 Pa. This demonstrates that the response of the IST-2018 sensor to pressure variations is almost as linear as that of the high quality MB2005 sensor. The intrinsic background noise of our sensor is less than 0.05 Pa RMS on average in the range [0.06 – 40] Hz on the 'IS' output and less than 1 Pa RMS on the

'MEMS' output. The amplitude ranges are ± 240 Pa and ± 1245 Pa for the 'IS' and the 'MEMS' outputs, respectively.

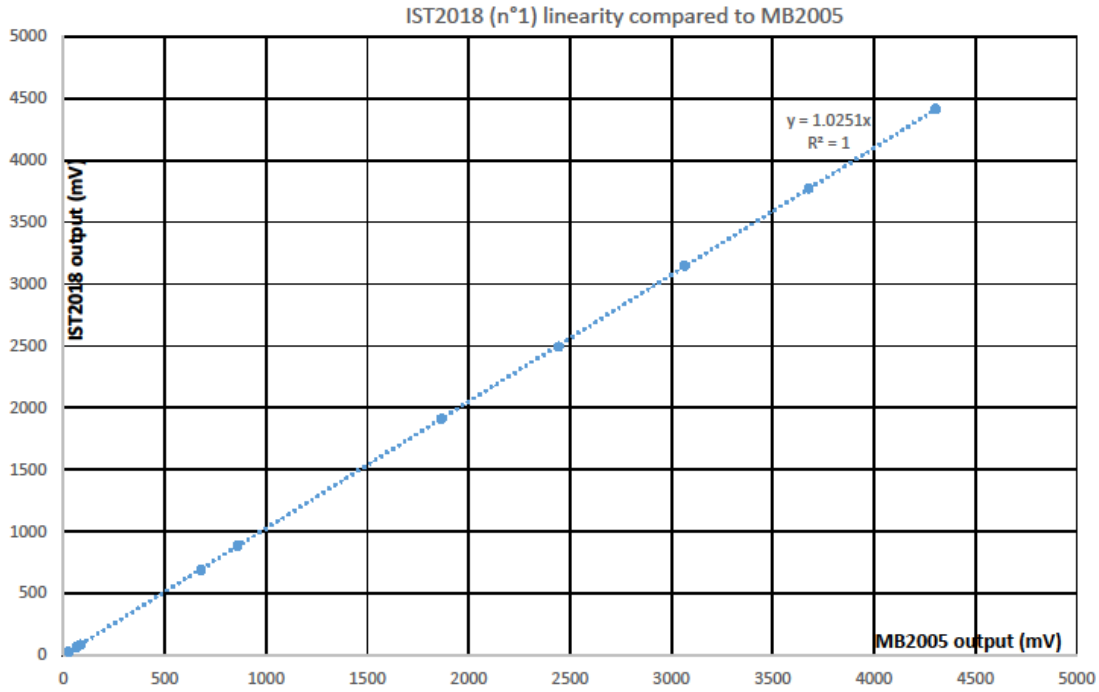

Figure 4. Comparison of amplitude variations measured by the MB2005 and the IST-2018 sensors, as a test of relative linearity of the later one.

Some types of sensor may be sensitive to mechanical oscillations. In this case, they must be carefully isolated from ground motions in order to avoid spurious output signals. We thus studied the sensitivity of our sensors to mechanical vibrations. We built a simple vibrating platform on which we set together the MB2005 and IST-2018 sensors and an accelerometer. We observed that, while the MB2005 is strongly sensitive to mechanical oscillations, the IST-2018 is not perturbed by vibrations. This implies that the later sensor can be fixed directly on the ground or even on trees without increasing its background noise. Appendix B gives more details on this experiment.

6. Field experiment

A team from the University of Liverpool, UK, and the Observatorio Volcanológico del INGEMMET, Peru, carried out a field experiment at Sabancaya volcano in March 2018. In order to compare them, they deployed a Chaparral Model 60 UHP and a IST-2018 infrasound sensor. The sensors were installed close to each other at a site located on top of a small hill

protected from the wind by some rocks; the site is ~6 km from the active crater, with direct view to the vent. Several explosions occurred during the experiment, producing ash plumes of up to 5000 m above the crater (BGVN, 2018). Figure 5 displays two examples of explosion recorded by the two instruments, and their respective spectra. A good agreement is generally obtained between the waveforms, the amplitudes and the spectra. However, for the explosion at 21:05, the record obtained by the IST-2018 sensor contains larger variations at low frequency. This is mainly due to the difference in the low corner frequency of the high-pass filter of the instruments used in this experiment, which were 30 and 7 mHz for the Chaparral and IST-2018, respectively. More field tests will be necessary to confirm the good functioning and calibration of the IST-2018 sensor.

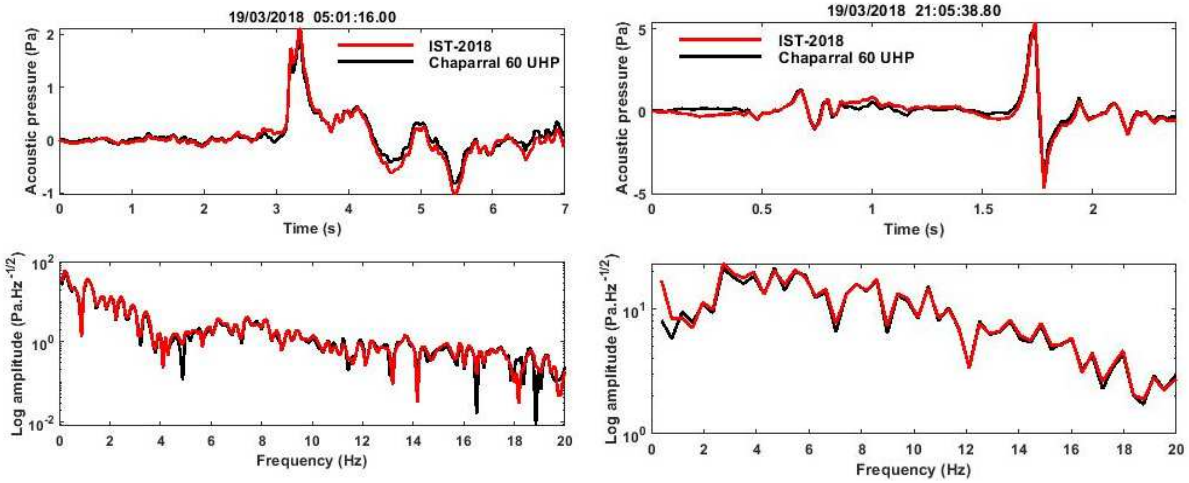

Figure 5. Comparison of waveforms and spectra of 2 explosions of Sabancaya volcano, Peru, recorded by a Chaparral 60 UHP and a IST-2018 collocated infrasound sensors.

7. Discussion

The characteristics of a sensor result from the balance between several constraints and from some technological choices. In our case, the main objectives were to produce a robust, low power, inexpensive, and well-calibrated infrasound sensor that can be easily connected to seismic acquisition devices. Thus, because the IST-2018 sensor is based on a microelectromechanical systems technology and uses a limited number of electronic components, some of its features are not as good as those of high quality instruments such as the Martec MB2005 and the Chaparral 60 UHP. For example, although it is well-adapted to detect most infrasound signals described in the literature, the smaller amplitude range of its 'IS' output may result in clipping records of strong explosions at short distance. In this case

the ‘MEMS’ output of the IST-2018 can be useful. However, the sensitivities and frequency ranges of these three sensors have similar values. The IST-2018 can also be compared with the BSU and the Gem sensors. The lower sensitivity and noise level of the latter two probably result from the lack of amplification or the use of a small gain amplifier in these devices. Nevertheless, the noise level of the IST-2018 could be reduced by using oversampling and averaging techniques. We plan to further reduce the input voltage, consumption and noise level by using new electronic components. The other characteristics of the three sensors – frequency and amplitude ranges, power – do not differ much. On the other hand, a IST-2018 sensor was installed very close to the Pisciarelli fumarole, Italy. During one year, it measured the acoustic level of a vent without failure, which is a good test of robustness in harsh and corrosive volcanic environments.

This infrasound sensor is relatively easy to build. The electronic boards are produced by a cabling company. The structure and packaging are made by 3D printer. In the lab, we prepare the capillary tube, assemble the different parts, finish the cabling to the connector, and we fill the case with resin. There are no major difficulties for a person with good technical skill. The longest task is to calibrate the sensors. This lab-made sensor is available for any volcano observatories and research groups at low cost (a few hundred euros, depending of the accessory devices delivered – power, breaking box, cables). The user manual of the IST-2018 presents a detailed description of the sensor, including specifications, cabling, and electrical connections. It gives some recommendations for field installations, such as the need of protection from direct solar radiation and from obstruction of the pneumatic inputs.

8. Conclusion

Many advancements in sciences resulted from improvements of instrumentation. In volcano seismology for example, the use of broadband seismometers allowed the discovery of new phenomena such as the very-long-period (VLP) events which are associated with mass movements in the plumbing system (Neuberg et al., 1994; Ohminato and Ereditato, 1997; Chouet and Matoza, 2013). The integration of acoustic sensors in permanent networks or in temporary deployments provides complementary observations to seismic records and improves the ability to understand some volcanic processes, such as Strombolian (Braun and Ripepe, 1993; Vergniolle and Brandeis, 1994) and Vulcanian eruptions (Johnson and Aster,

2005; Valade et al., 2012), and to reduce the related risks, for example by detecting pyroclastic density currents or rock fall (Jones and Johnson, 2011). The infrasound sensor IST-2018 we have developed and presented in this paper is well suited to the measurements of acoustic waves produced by volcanoes. It is characterized by broad frequency band, high dynamic range, low noise level and low power consumption. It is designed to work in harsh environmental conditions after easy installation. The careful determination of its transfer function and sensitivity with the especially designed calibration system makes the IST-2018 sensor a true instrument for the measurement of acoustic phenomena. Its low cost and easy connection to most seismic digitizers may foster its use in many monitoring networks and acoustic arrays on volcanoes, as well as for a large variety of applications.

Acknowledgements

The development of the infrasound sensor has been supported by grants from Labex OSUG@2020 (Investissements d'avenir – ANR10 LABX56) and from AAP Université Savoie Mont Blanc. We would like to thank Silvio De Angelis, Alejandro Díaz Moreno and Roger Machacca for carrying out the field experiment at Ubinas volcano and for sharing their data. We are indebted to Jean Vandemeulebrouck for his useful and encouraging advices and for improving the manuscript. We also thank two anonymous reviewers for their useful comments.

References

Anderson, J.F., Johnson, J.B., Bowman, D.C. and Ronan, T.J., 2018. The Gem Infrasound Logger and Custom-Built Instrumentation. Seismol. Res. Lett., 89(1): 153-164.

Bowman, J.R., Baker, G.E. and Bahavar, M., 2005. Ambient infrasound noise. Geophys. Res. Lett., 32: L09803.

Braun, T. and Ripepe, M., 1993. Interaction of seismic and air waves recorded at Stromboli volcano. Geophys. Res. Lett., 20(1): 65-68.

Chouet, B.A. and Matoza, R.S., 2013. A multi-decadal view of seismic methods for detecting precursors of magma movement and eruption. J. Volcanol. Geotherm. Res., 252: 108-175.

De Angelis, S., Fee, D., Haney, M. and Schneider, D., 2012. Detecting hidden volcanic explosions from Mt. Cleveland Volcano, Alaska with infrasound and ground-coupled airwaves. Geophys. Res. Lett., 39(21): GL053635.

Delclos, C., Blanc, E., Broche, P., Glangeaud, F., and Lacoume, J.L., 1990. Processing and interpretation of microbarograph signals generated by the explosion of Mount St. Helens. J. Geophys. Res., 95, 5485–5494.

Fee, D. and Matoza, R., 2013. An overview of volcano infrasound: From hawaiian to plinian, local to global. J. Volcanol. Geotherm. Res., 249: 123-139.

Garcés, M., Fee, D., and Matoza, R., 2013. Volcano acoustics. *In* Fagents S., Gregg T., & Lopes R., Modeling volcanic processes: The Physics and Mathematics of Volcanism, pp. 359-382. Cambridge University

Global Volcanism Program, 2018. Report on Sabancaya (Peru). In: Venzke, E (ed.), Bulletin of the Global Volcanism Network, 43:6. Smithsonian Institution.

Johnson, J.B. and Aster, R.C., 2005. Relative partitioning of acoustic and seismic energy during Strombolian eruptions. J. Volcanol. Geotherm. Res., 148: 334-354.

Johnson, J.B., Lees, J. and Varley, N., 2011. Characterizing complex eruptive activity at Santiaguito, Guatemala using infrasound semblance in networked arrays. J. Volcanol. Geotherm. Res., 199(1-2): 1-14.

Johnson, J.B. and Ripepe, M., 2011. Volcano infrasound: a review. J. Volcanol. Geotherm. Res., 206: 61-69.

Jones, K.R. and Johnson, J.B., 2011. Mapping complex vent eruptive activity at Santiaguito, Guatemala using network infrasound semblance. J. Volcanol. Geotherm. Res., 199(1-2): 15-24.

Kromer, R. P., and McDonald, T. S., 2000. Infrasound sensor models and evaluation. Proc. 22nd Annual DoD/DOE Seismic Research Symp.: Planning for Verification of and Compliance with the Comprehensive Nuclear-Test-Ban Treaty, New Orleans, LA, Department of Defense and Department of Energy. [Available online at http://handle.dtic.mi1/100.2/ADA523399.]

Kromer, R.P., Hart, D. M. and Harris, J. M., 2007. Test definitions for the evaluation of infrasound sensors. Sandia National Laboratories Tech. Rep. SAND2007-5038, 11 pp. [Available online at http://prod.sandia.gov/techlib/access-control.cgi/2007/075038.pdf.]

Le Pichon, A., Blanc, E. and Hauchecorne, A. (Eds), 2010. Infrasound monitoring for atmospheric studies. Springer, New York.

Marcillo, O., Johnson, J.B. and Hart, D., 2012. Implementation, Characterization, and Evaluation of an Inexpensive Low-Power Low-Noise Infrasound Sensor Based on a Micromachined Differential Pressure Transducer and a Mechanical Filter. J. Atmosph. Oceanic Technol., 29(9): 1275-1284.

Mentink, J.H. and Evers, L.G., 2011. Frequency response and design parameters for differential microbarometets. J. Acoust. Soc. Am., 130: 33-41.

Neuberg, J., Luckett, R., Ripepe, M. and Braun, T., 1994. Highlights from a seismic broadband array on Stromboli volcano. Geophys. Res. Lett., 21(9): 749-752.

Ohminato, T. and Ereditato, D., 1997. Broadband seismic observations at Satsuma-Iwojima volcano, Japan. Geophys. Res. Lett., 24(22): 2845-2848.

Ponceau, D. and Bosca, L., 2010. Low-noise broadband microbarometers. *In*: A. Le Pichon, E. Blanc and A. Hauchecorne (Editors), Infrasound monitoring for atmospheric studies. Springer, New York, pp. 119-140.

Richiardone, R., 1993. The transfer function of a differential microbarometer. J. Atmosph. Oceanic Technol., 10: 624-628.

Rocard, Y., 1971. Demande de brevet pour procédé et dispositif de détection et d'enregistrement des variations de la pression atmosphérique. DAM/DIREX 0417.

Valade, S., Donnadieu, F., Lesage, P., Mora, M.M., Harris, A. and Alvarado, G.E., 2012. Explosion mechanisms at Arenal volcano, Costa Rica: An interpretation from integration of seismic and Doppler radar data. J. Geophys. Res., 117(B1): B01309.

Vergniolle, S., Brandeis, G. and Mareschal, 1996. Strombolian explosions. 2. Eruption dynamics determined from acoustic measurements. J. Geophys. Res., 101(B9): 20449-20466.

Walker, K.T., and Hedlin, M.A.H., 2010. A review of wind-noise redaction methodologies. *In*: A. Le Pichon, E. Blanc and A. Hauchecorne (Editors), Infrasound monitoring for atmospheric studies. Springer, New York, pp. 141-182.

Appendix A

To calibrate our sensors, we have developed two generators of sinusoidal pressure variations operating in the frequency ranges from 1 mHz to 10 Hz, and from 5 Hz to 10 kHz, respectively. Each generator consists of a variable volume chamber connected in a closed circuit to reference sensors and to the sensor to calibrate. At each measuring point, the chamber is equilibrated to the atmospheric pressure and then the pressure oscillations are generated at the desired frequency.

A1. Variable pressure generator from 1 mHz to 10 Hz

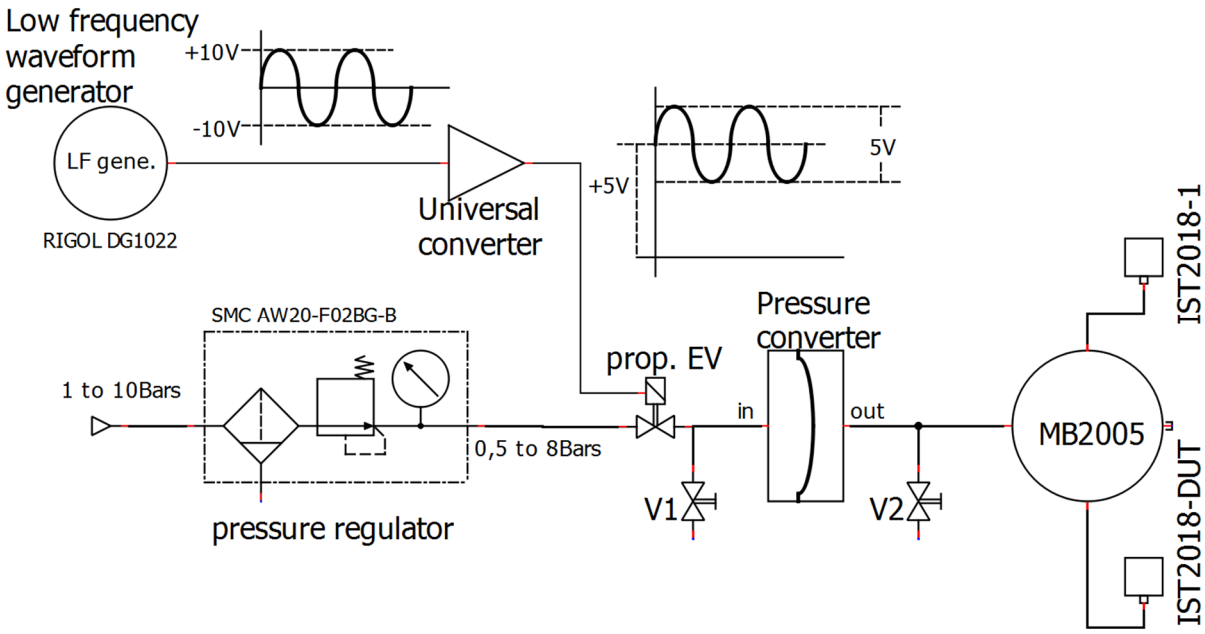

Figure A1. Block diagram of the 'low-frequency' calibration system

The variable volume chamber is the right part of the module 'Pressure converter' (figure A1). This module converts the strictly positive inlet pressure into pressurization and depressurization around the equilibrium pressure which is set at the beginning of the measurement by means of valve V2. It consists of two cylindrical chambers connected by an elastic membrane. The modulation pressure, generated by the proportional solenoid valve (prop. EV), is applied in the left part of the module. This solenoid valve is powered by the pressure regulator (SMC AW20-F02NG-B) and controlled by a Low-Frequency generator (RIGOL DG1022) through a universal voltage converter. The reference sensors IST2018-1 and MB2005 and the sensor to calibrate IST2018-DUT are connected in closed circuit (valve V2 closed) to the output of the pressure converter (figure A2).

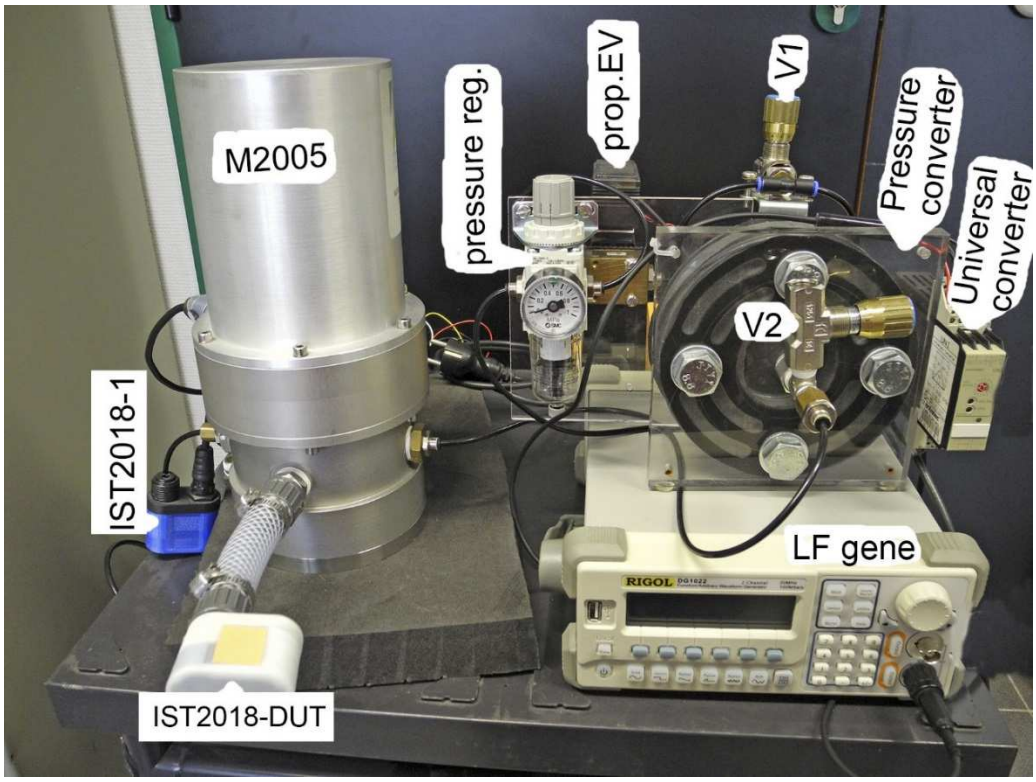

Figure A2. Picture of the 'low-frequency' calibration device displaying the pressure converter on the top of the Low-frequency Generator, the valves, and the three sensors.

The signal obtained is very close to a sine wave (figure A3). It does not have breaks that would make calibration difficult.

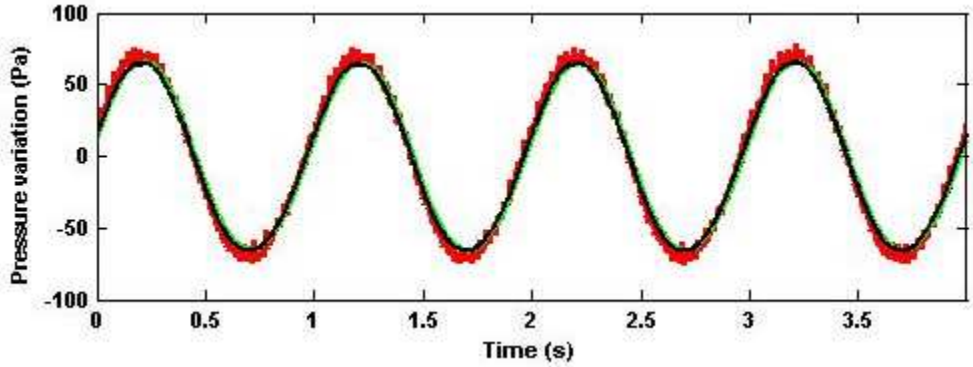

Figure A3. Example of sinusoidal signals recorded by the two reference sensors MB2005 (green) and IST2018-1 (red, not filtered) and the IST-2018 to calibrate (black). Here the input pressure varies in the range +75 Pa/-55 Pa at a frequency of 1 Hz.

A2. Variable pressure generator from 5 Hz to 10 kHz

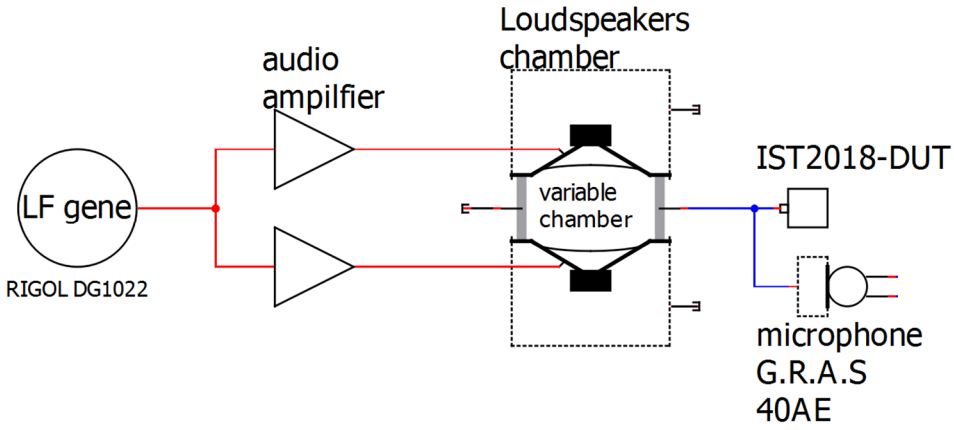

Figure A4. Block diagram of the 'high-frequency' calibration system

The variable volume chamber consists of a cylinder closed at each end by waterproof speakers (figure A4). The movement of the loudspeaker diaphragms creates the pressure modulation. A low-frequency generator (RIGOL DG1022) controls each loudspeaker by means of an audio amplifier. The variable volume chamber has two pneumatic outlets. The left outlet has a plug for balancing with atmospheric pressure. On the right output, a GRAS 40AE microphone, which is the reference sensor, and the sensor to calibrate IST2018-DUT are connected in closed circuit (figure A5).

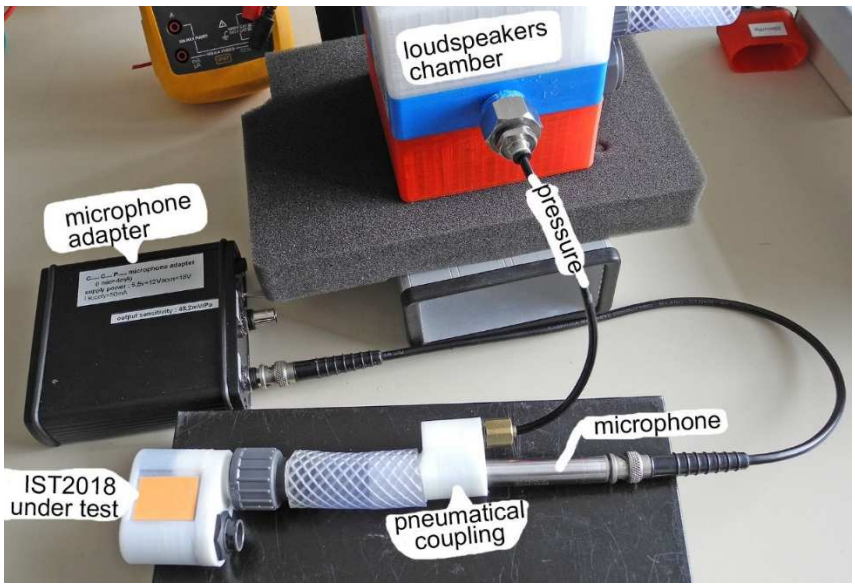

Figure A5. Picture of the 'high-frequency' calibration device displaying the loudspeaker chamber (top), the reference microphone, and the IST-2018 sensor to calibrate.

In summary, the principle and design of these two calibration devices are simple and their cost is modest. They can be built easily in a research laboratory. They result easy to use and

efficient to calibrate infrasound sensors. The accuracy of the calibration depends mainly on the quality of the reference sensors used as standard.

Appendix B

In order to study the sensitivity of the sensors to mechanical vibrations, we fixed together an accelerometer, an IST-2018, and a MB2005 sensors. We placed this equipment on a plastic canister that is used as a vibrating platform ("vibrator" in figure B1). Through the proportional solenoid valve, "prop. EV", we sent a variable pressure into the canister, which made it vibrate. These vibrations were thus transmitted synchronously to all sensors.

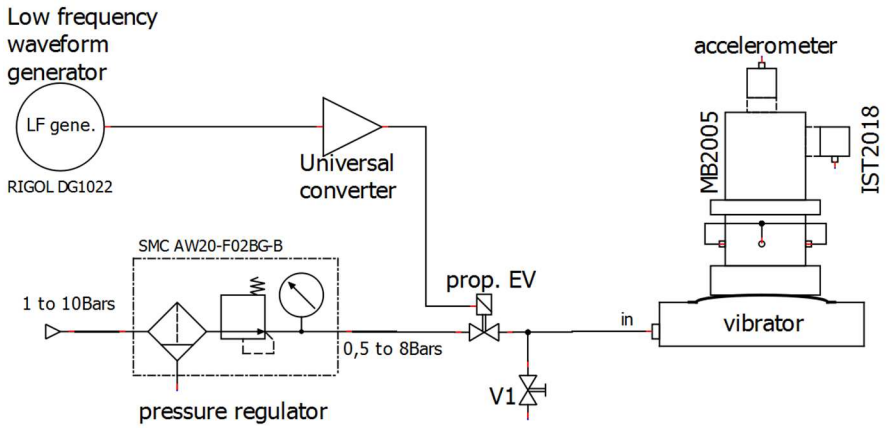

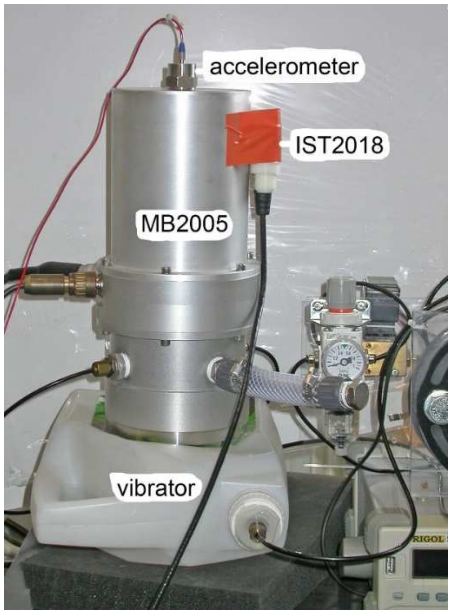

Figure B1. Block diagram (top) and picture (bottom) of the vibrations generator.

We generated sinusoidal vertical accelerations with frequencies from 1 to 40 Hz and amplitudes from 0.15 to 1.5 10^{-2} m s^{-2} and recorded the output signals of both MB2005 and

IST-2018 sensors. Figure B2 displays the sensors responses to sinusoidal accelerations of frequency 10 Hz and amplitude 1.5 10^{-2} m s^{-2}. The MB2005 produces a sinusoidal pressure variation with amplitude of 8 Pa, while the IST-2018 generates an aleatory signal of 0.024 Pa RMS, the same level as that of the signal obtained when no mechanical vibrations are applied on. The obtained sensitivity of the MB2005 to mechanical vibrations varies from 800 to 350 Pa/(m s^{-2}) for frequencies from 1 to 40 Hz. The IST-2018 is almost insensitive to the vibrations in the three spatial directions.

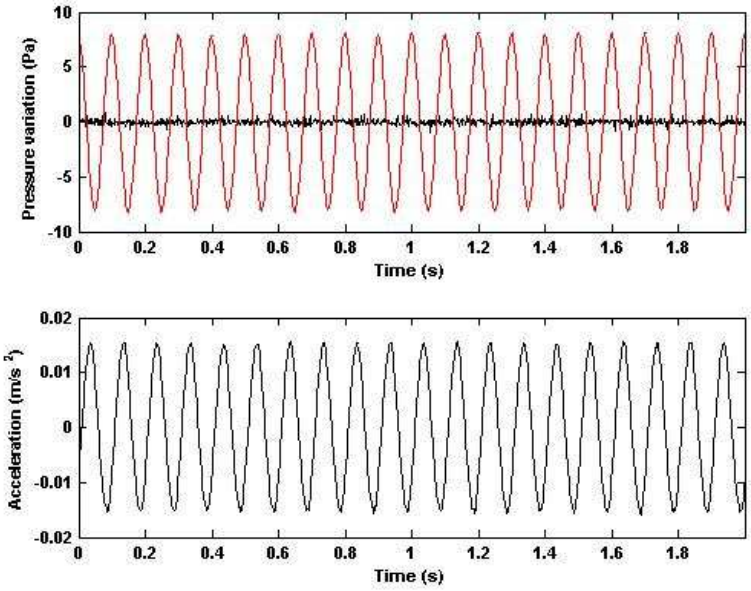

Figure B2. Response of the infrasound sensors to sinusoidal vertical mechanical vibrations of frequency 10 Hz. Top panel: outputs of the MB2005 (red) and IST-2018 (black, multiplied by 10) sensors. Bottom panel: corresponding acceleration. The output levels of IST-2018 with and without mechanical vibrations are identical.